tremely sparse, thus allowing a very high time and memory efficiency. The number of examples presented show a very good agreement with previous studies and guarantee the general applicability of the method. Finally, the last example is intended to serve as a reference for later analyses.

APPENDIX

Definition of the submatrices involved in (9):

$$M_1 = \iint_S (-VW_{x1}^T + UW_{y1}^T)\,dS \tag{A1}$$

$$M_2 = \iint_S [-VW_{x2}^T + UW_{y2}^T + (V_x - U_y)W_{z1}^T]\,dS \tag{A2}$$

$$M_3 = \iint_S (V_x - U_y)W_{z2}^T\,dS \tag{A3}$$

$$M_4 = \iint_S (-VW_{x3}^T + UW_{y3}^T)\,dS \tag{A4}$$

$$M_5 = \iint_S (V_x - U_y)W_{z3}^T\,dS \tag{A5}$$

$$M_6 = \iint_S (N_yW_{x1}^T - N_xW_{y1}^T)\,dS \tag{A6}$$

$$M_7 = \iint_S (N_yW_{x2}^T - N_xW_{y2}^T)\,dS \tag{A7}$$

$$M_8 = \iint_S (N_yW_{x3}^T - N_xW_{y3}^T)\,dS \tag{A8}$$

where

$$W_{x1}^T = (\hat{\mu}^{-1})_{xx}V^T - (\hat{\mu}^{-1})_{xy}U^T \tag{A9}$$

$$W_{y1}^T = (\hat{\mu}^{-1})_{yx}V^T - (\hat{\mu}^{-1})_{yy}U^T \tag{A10}$$

$$W_{z1}^T = (\hat{\mu}^{-1})_{zx}V^T - (\hat{\mu}^{-1})_{zy}U^T \tag{A11}$$

$$W_{x2}^T = (\hat{\mu}^{-1})_{xz}(V_x^T - U_y^T) \tag{A12}$$

$$W_{y2}^T = (\hat{\mu}^{-1})_{yz}(V_x^T - U_y^T) \tag{A13}$$

$$W_{z2}^T = (\hat{\mu}^{-1})_{zz}(V_x^T - U_y^T) \tag{A14}$$

$$W_{x3}^T = (\hat{\mu}^{-1})_{xx}N_y^T - (\hat{\mu}^{-1})_{xy}N_x^T \tag{A15}$$

$$W_{y3}^T = (\hat{\mu}^{-1})_{yx}N_y^T - (\hat{\mu}^{-1})_{yy}N_x^T \tag{A16}$$

$$W_{z3}^T = (\hat{\mu}^{-1})_{zx}N_y^T - (\hat{\mu}^{-1})_{zy}N_x^T. \tag{A17}$$

Finally,

$$N_1 = \iint_S [U(\varepsilon_{xx}U^T + \varepsilon_{xy}V^T) + V(\varepsilon_{yx}U^T + \varepsilon_{yy}V^T)]\,dS \tag{A18}$$

$$N_2 = \iint_S (\varepsilon_{xz}UN^T + \varepsilon_{yz}VN^T)\,dS \tag{A19}$$

$$N_3 = \iint_S N(\varepsilon_{zx}U^T + \varepsilon_{zy}V^T)\,dS \tag{A20}$$

$$N_4 = \iint_S \varepsilon_{zz}NN^T\,dS. \tag{A21}$$

REFERENCES

[1] K. Hayata, K. Miura, and M. Koshiba, "Full vectorial finite element formalism for lossy anisotropic waveguides," *IEEE Trans. Microwave Theory Tech.*, vol. 37, pp. 875–883, May 1989.

[2] K. D. Paulsen and D. R. Lynch, "Elimination of vector parasites in finite element Maxwell solutions," *IEEE Trans. Microwave Theory Tech.*, vol. 39, pp. 395–404, Mar. 1991.

[3] R. Miniowitz and J. P. Webb, "Covariant-projection quadrilateral elements for the analysis of waveguides with sharp edges," *IEEE Trans. Microwave Theory Tech.*, vol. 39, pp. 501–505, Mar. 1991.

[4] I. Bardi and O. Biro, "An efficient finite-element formulation without spurious modes for anisotropic waveguides," *IEEE Trans. Microwave Theory Tech.*, vol. 39, pp. 1133–1139, July 1991.

[5] Y. Lu and F. A. Fernandez, "An efficient finite element solution of inhomogeneous anisotropic and lossy dielectric waveguides," *IEEE Trans. Microwave Theory Tech.*, vol. 41, pp. 1215–1223, June/July 1993.

[6] L. Nuño, J. V. Balbastre, J. Igual, M. Ramón and M. Ferrando, "Analysis of inhomogeneous and anisotropic waveguides by the finite element method," in *2nd Topical Mtg. Elect. Performance Electron. Packaging*, Monterey, CA, Oct. 20–22, 1993, pp. 47–49.

[7] Z. J. Cendes, "Vector finite elements for electromagnetic field computation," *IEEE Trans. Magn.*, vol. 27, pp. 3958–3966, Sept. 1991.

[8] J. F. Lee, D. K. Sun, and Z. J. Cendes, "Tangential vector finite elements for electromagnetic field computation," *IEEE Trans. Magn.*, vol. 27, pp. 4032–4035, Sept. 1991.

[9] M. Koshiba and K. Inoue, "Simple and efficient finite-element analysis of microwave and optical waveguides," *IEEE Trans. Microwave Theory Tech.*, vol. 40, pp. 371–377, Feb. 1992.

[10] B. M. Dillon and J. P. Webb, "A comparison of formulations for the vector finite element analysis of waveguides," *IEEE Trans. Microwave Theory Tech.*, vol. 42, pp. 308–316, Feb. 1994.

[11] Y. Lu and F. A. Fernandez, "Vector finite element analysis of integrated optical waveguides," *IEEE Trans. Magn.*, vol. 30, pp. 3116–3119, Sept. 1994.

[12] B. C. Anderson and Z. J. Cendes, "Solution of ferrite loaded waveguide using vector finite elements," *IEEE Trans. Magn.*, vol. 31, pp. 1578–1581, May 1995.

Some Characteristics of Ridge-Trough Waveguide

Debatosh Guha and Pradip Kumar Saha

***Abstract*—A single-ridged waveguide with a symmetrical longitudinal trough below the ridge, designated as a ridge-trough waveguide (RTW) has been recently proposed as a wafer probe. The authors have theoretically calculated the cutoff, bandwidth, and impedance characteristics of this modified single-ridged waveguide in two different configurations using the Ritz–Galerkin technique and different domain decompositions. The results indicate that a RTW can be a low impedance broad-band structure.**

***Index Terms*—Low impedance broad-band waveguide.**

I. INTRODUCTION

In recent years microwave researchers have been paying attention to developing transitions between the coplanar waveguide (CPW) and other microwave transmission media for efficient utilization of some of the advantages of the CPW (one of which is its suitability in the design of microwave wafer probes [1]). A few rectangular waveguides to CPW transitions have been reported which utilize finline transitions [2], [3], modified ridged waveguides [4], [5], and some other configurations [6], [7].

Of these structures, the ridge-trough waveguide (RTW) [5] has attracted the authors' attention, prompting them to analyze rectangular waveguides with ridges and shaped septa which promise broad-

Manuscript received August 22, 1995; revised November 21, 1996.

The authors are with the Institute of Radio Physics and Electronics, University of Calcutta, 700 009 Calcutta, India.

Publisher Item Identifier S 0018-9480(97)01714-6.

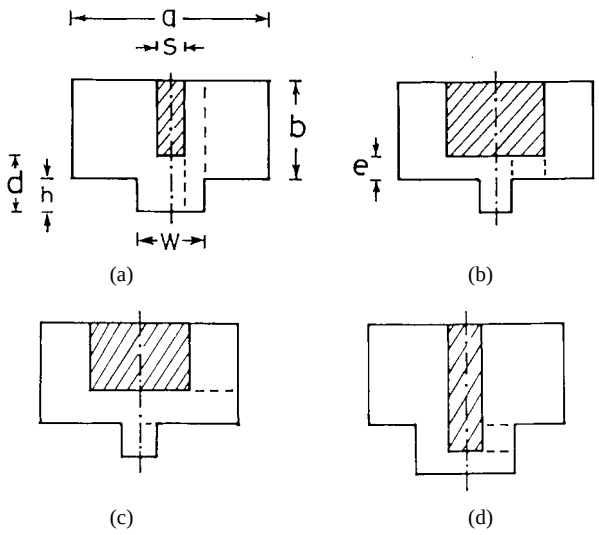

Fig. 1. Cross-sectional views of the RTW in different configurations. Broken lines indicate the aperture planes over which fields are matched. (a) Ridge narrower than trough: configuration C1, formulation F1, (b) ridge wider than trough: configuration C2, formulation F2, (c) configuration C2, formulation F3, and (d) configuration C1, formulation F4.

band transmission characteristics. The RTW is another variant of the conventional single-ridged guide (SRG) in which a centered longitudinal trough is introduced on the broadwall below the ridge. In [5], the RTW has been suggested in two configurations, shown in Fig. 1(a) and (b). Only Fig. 1(a) has been studied experimentally as the wafer probe. Quasi-static models of the RTW for calculating the cutoff frequency and characteristic impedance of the lowest mode are presented in [5].

The authors have theoretically determined the cutoff, bandwidth, and impedance characteristics of the lowest TE mode of the RTW to explore if it can be used as another broad-band transmission line. The RTW appears to be suitable as broad-band mounts for active and passive devices. The authors' analysis is based on the Ritz–Galerkin technique which is well suited to such configurations. Due to the nature of the cross-sectional shape, the domain decomposition for application of the technique can be done in several ways. This will be discussed in the next section. There are very few results available in the literature with which the authors' data can be compared. Nevertheless, the authors present their theoretical data as these are new and should be useful in the design of the RTW.

II. RTW and Formulation of Eigenvalue Problem

The cross-sectional geometry of the RTW in two different configurations is shown in Fig. 1(a) and (b). In the configuration of Fig. 1(a), the ridge is always narrower than the trough ($s < w$) and, hence, may penetrate the trough region leaving gap d at the bottom, as in Fig. 1(d). This will be referred to as configuration C1. Fig. 1(a) also shows one way of dividing the cross-sectional area (actually half the area with a magnetic or electric symmetry plane along the center line) which the authors shall refer to as formulation F1. The broken lines indicate the aperture planes over which the subregional fields are matched. Thus, F1 can solve only the structures having $s < w$, but any gap height d relative to the trough depth h.

In Fig. 1(b), the ridge is always wider than the trough ($s > w$). This configuration will be referred to as C2 and the domain decomposition indicated will be referred to as formulation F2. For this configuration an additional dimensional parameter e is introduced only for convenience of presenting the numerical data. Fig. 1(c) shows the configuration C2 with another possible formulation, F3, which encompasses configuration C1 as well but for $d > h$ only. Fig. 1(d) shows the configuration C1 with formulation F4 which can solve only the case of the ridge inside the trough ($d < h$).

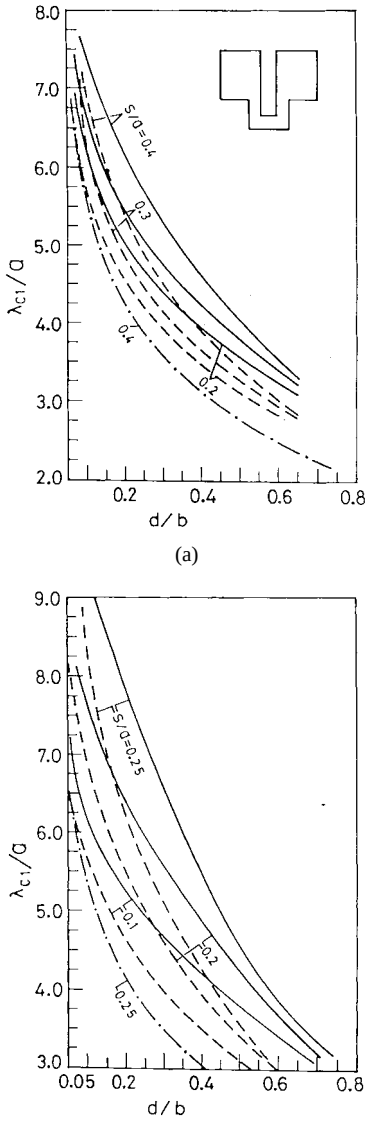

Fig. 2. Normalized cutoff wavelength λ_{c1}/a of the RTW versus normalized gap height $d/b.b/a = 0.45$,—— $h/b = 0.4$, – – – – $h/b = 0.2$, –.–.–. SRG (a) $w/a = 0.5$, and (b) $w/a = 0.3$.

Using these formulations, the TE eigenvalue equations have been derived and solved for calculating the cutoff wavelengths of the lowest and the first higher order TE modes from which the bandwidth is determined. As the analysis is straightforward and the procedure well documented (e.g., [8]–[11]), only the results of numerical computation are presented. The gap-impedance data are also given for the configuration C1 using the subregional fields of the formulation F1.

III. Numerical Results and Discussion

The authors have mentioned four possible ways of dividing the cross section and each formulation is capable of solving certain configurations. The authors have carried out numerical calculations using all four formulations mainly because it is not possible to compare their results against some standard or known structures except the single-ridged waveguide for which the trough itself is

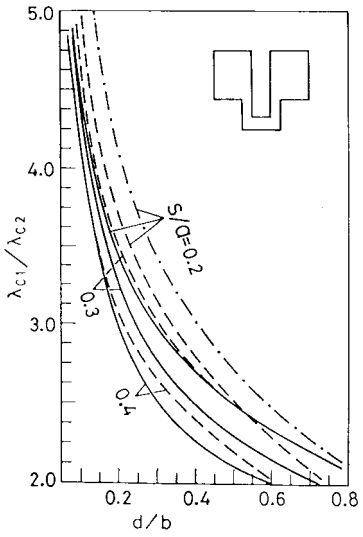

(a)

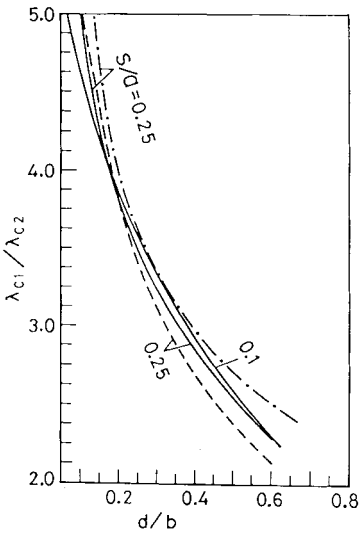

(b)

Fig. 3. Bandwidth $\lambda_{cl}/\lambda_{c2}$ versus d/b. All parameters and denotations as in Fig. 2. (a) $w/a = 0.5$ and (b) $w/a = 0.3$.

TABLE I
NORMALIZED CUTOFF WAVELENGTH FOR RIDGE INSIDE THE TROUGH COMPUTED FROM TWO DIFFERENT FORMULATIONS. $b/a = 0.45, h/b = 0.4$

		λ_{c1}/a					
		From : F1			From : F4		
d/b	*s/a*	*w/a*			*w/a*		
		0.3	0.4	0.5	0.3	0.4	0.5
	0.1	7.26	6.75	6.64	7.28	7.35	7.63
	0.25	10.25	9.39	8.04	9.82	8.33	8.30
0.05	0.35		10.47	8.69		9.82	8.61
	0.4			9.13			8.89
	0.1	4.72	4.27	4.05	4.49	4.18	4.04
	0.25	6.75	5.06	4.52	6.12	4.78	4.39
0.3	0.35		6.46	4.95		5.86	4.69
	0.4			5.32			4.96

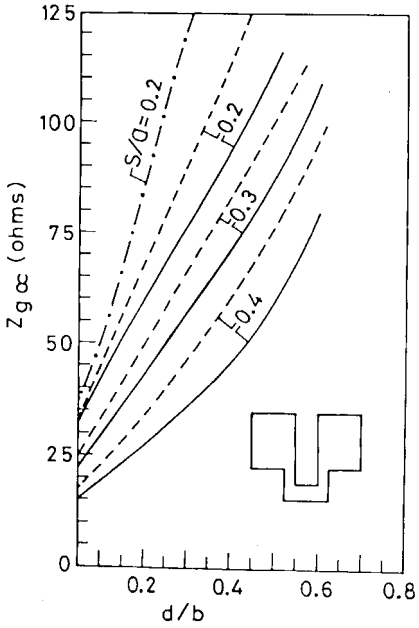

Fig. 4. Gap impedance at infinite frequency $Z_{g\infty}$ versus normalized gap height d/b. $b/a = 0.45$, $w/a = 0.5$, —— $h/b = 0.4$, – – – – $h/b = 0.2$, –.–.–. SRG.

made to vanish in the limit. As will be observed below, the results obtained from different formulations do not always have close mutual agreement. The reason for such discrepancies for certain configurations and certain dimensions is the nature of domain decomposition (although in each case the relative convergence effect was found to be insignificant). It is well known, and an inspection of Fig. 1(a)–(d) will also reveal, that while writing the fields in the different domains as summations of mode functions in separable forms with unknown amplitude coefficients, it is not possible, in general, to exactly satisfy *a priori* the boundary conditions on all the waveguide walls. Clearly this happens when at least one boundary of a domain is a longitudinal discontinuity plane containing both conducting walls as well as interfaces between adjacent domains. Fulfillment of the boundary conditions on these conducting walls is enforced in the formulation while applying the continuity of fields over the apertures and expressing the unknown coefficients in terms of the unknown aperture electric fields. The numerical results thus obtained show that the vanishing of the tangential electric field is not exactly satisfied over the conducting walls of the discontinuity planes. Matching of the TE fields over the apertures was also examined from the computed field components. The pattern of the TE fields varies with the ridge and trough dimensions as does the degree of matching for the same number of field expansion terms. As such, one particular formulation can not be conclusively accredited with the best accuracy for all dimensions.

A. Ridge Narrower than Trough (Configuration C1)

In Fig. 2(a) and (b), the normalized cutoff wavelength λ_{c1}/a of the lowest TE mode is shown as a function of the ridge gap d/b with the ridge width s/a as a parameter for two sets of trough dimensions. The graphical data obtained from formulation F1 are also presented in tabular form in Table I for comparison of some spot values with those obtained from formulation F4. It is noted that the difference in the values obtained from the formulations F1 and F4 is significant for some cases of wide ridges and narrow troughs.

An examination of Fig. 2(a) and (b) and the available SRG data brings out the following features.

1 For normalized gap height of $d/b = 0.1$, as an example, the SRG shows a maximum value of 5.6 of λ_{c1}/a at $s/a = 0.4$.

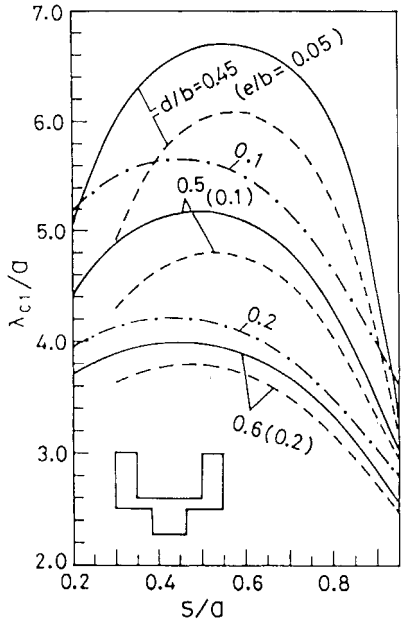

(a)

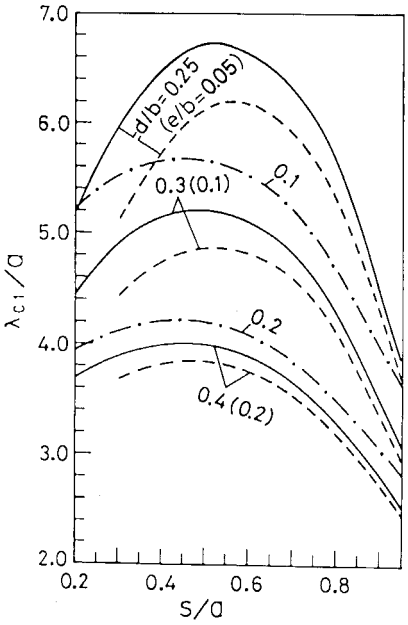

(b)

Fig. 5. Normalized cutoff wavelength λ_{c1}/a versus normalized ridge width s/a. $b/a = 0.45$, —— $w/a = 0.2$, – – – – $w/a = 0.3$, –.–.– SRG. (a) $h/b = 0.4$. (b) h/b.

Thus, substantially higher cutoff wavelength of the lowest TE mode can be realized with RTW having the ridge inside the trough.

2 For a particular ridge width s/a, a narrow trough is more effective in increasing λ_{c1}/a than a wider trough, the trough depth remaining the same.

The maximum bandwidth $\lambda_{c1}/\lambda_{c2}$, where λ_{c2} is the cutoff wavelength of the first-order TE mode, available in the configuration C1, is, however, a little lower than that of the SRG with the same s/a. This can be seen from the data presented in Fig. 3(a) and (b), computed with formulation F1. The figure show how the bandwidth decreases as a ridge, initially inside the trough with a small gap at the bottom, is withdrawn up and out of the trough.

TABLE II
NORMALIZED CUTOFF WAVELENGTH FOR RIDGE WIDER THAN TROUGH COMPUTED FROM TWO DIFFERENT FORMULATIONS. $b/a = 0.45, h/b = 0.4$

		λ_{c1}/a					
		From : F2			From : F3		
d/b	*s/a*	*w/a*			*w/a*		
		0.2	0.3	0.4	0.2	0.3	0.4
0.5 (*e/b*=0.1)	0.3	4.85			5.56		
	0.4	5.11	4.64		5.60	5.11	
	0.5	5.18	4.79	4.36	5.50	5.11	4.65
	0.6	5.08	4.76	4.40	5.34	5.10	4.80
	0.7	4.88	4.53	4.24	4.90	4.62	4.33
0.6 (*e/b*=0.2)	0.3	3.90			4.24		
	0.4	4.00	3.77		4.20	4.00	
	0.5	4.00	3.80	3.58	4.12	3.93	3.71
	0.6	3.89	3.72	3.53	3.99	3.83	3.67
	0.7	3.67	3.53	3.37	3.70	3.56	3.40

The gap-impedance characteristics, calculated on a power-voltage basis for a ridge narrower than the trough, is shown in Fig. 4, together with one SRG curve for comparison. The impedance expectedly increases with increasing gap height d/b with other parameters remaining constant. Introduction of the trough considerably lowers the gap impedance compared to the SRG values. Also, a deeper trough is more effective for realizing low impedance values than a shallow trough. Furthermore, in comparison with the SRG for which one has two ridge parameters to adjust, there are four ridge and trough parameters in the RTW; these being w/a, h/b, d/b, and s/a, allowing for an achievement of a desired impedance level with more flexibility.

B. Ridge Wider than Trough (Configuration C2)

This configuration is more amenable to comparison with the SRG since with vanishing of the trough the parameter e/b (where $d = h + e$, $e \neq 0$) reduces to the ridge gap parameter d/b of the single-ridged waveguide. Thus, the effect of incorporation of a trough below the ridge can be directly observed from the data. The cutoff wavelengths, computed from the formulations F2 and F3 are presented in Table II. The agreement between the two sets of data is much better than in case of configuration C1. The cutoff wavelengths as obtained from formulation F2 are also presented in Fig. 5(a) and (b). The bandwidth characteristics of this configuration are shown in Fig. 6(a) and (b). In general, introduction of a trough of a width less than the ridge width has detrimental effect on both the cutoff and bandwidth of the guide, and the effect is worse for wider troughs. This is to be expected since a wide trough below a ridge makes the structure look like a SRG with the same s/a but larger d/b.

IV. CONCLUSION

The authors have examined the cutoff, bandwidth, and impedance characteristics of the RTW recently developed for waveguide to CPW transition. From the authors' theoretical results, the RTW in the particular configuration of a ridge narrower than, and penetrating, the trough appears attractive for applications requiring low impedance levels. The bandwidth of the RTW in this configuration falls short of

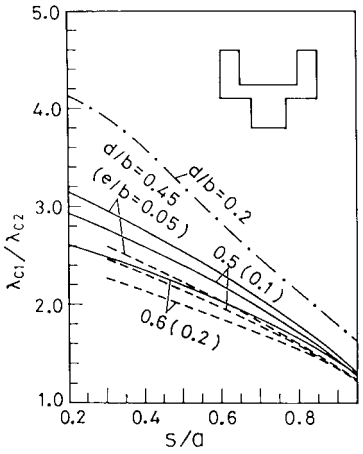

(a)

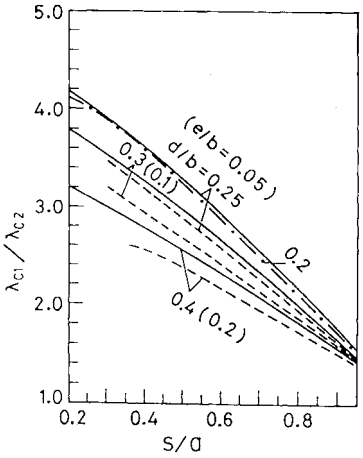

(b)

Fig. 6. Bandwidth $\lambda_{c1}/\lambda_{c2}$ versus s/a. All parameters and denotations as in Fig. 5. (a) $h/b = 0.4$ and (b) $h/b = 0.2$.

the SRG bandwidth, but the cutoff wavelength can be substantially larger. Thus, the properly designed RTW can be a broad-band low-impedance transmission medium. The RTW in the other configuration with a ridge wider than the trough appears less useful because the trough lowers both the cutoff wavelength and bandwidth.

References

[1] K. E. Jones, E. W. Strid, and K. R. Gleason, "Mm-wave wafer probes span 0 to 50 GHz," *Microwave J.*, vol. 30, no. 4, pp. 177–183, 1987.

[2] G. Begemann, "An X-band balanced finline mixer," *IEEE Trans. Microwave Theory Tech.*, vol. MTT-26, pp. 1007–1011, 1978.

[3] J. V. Bellantoni, R. C. Compton, and H. M. Levy, "A new W-band coplanar waveguide text fixture," in *1989 IEEE MTT-S Int. Microwave Symp. Dig.*, pp. 1203–1204.

[4] G. E. Ponchak and R. N. Simons, "A new rectangular waveguide to coplanar waveguide transition," in *IEEE MTT-S Int. Microwave Symp. Dig.*, vol. I, Dallas, TX, May 8–10, 1990, pp. 491–493.

[5] E. M. Godshalk, "A V-band wafer probe using ridge-trough waveguide," *IEEE Trans. Microwave Theory Tech.*, vol. 39, pp. 2218–2228, Dec. 1991.

[6] R. N. Simons, "New channelised coplanar waveguide to rectangular waveguide post and slot couplers," *Elec. Lett.*, vol. 27, no. 10, pp. 856–857, 1991.

[7] R. N. Simons and S. R. Taub, "New coplanar waveguide to rectangular waveguide end launcher," *Elec. Lett.*, vol. 28, no. 12, pp. 1138–1139, June 4, 1992.

[8] J. P. Montgomery, "On the complete eigenvalue solution of ridged waveguide," *IEEE Trans. Microwave Theory Tech.*, vol. MTT-19, pp. 547–555, June, 1971.

[9] D. Dasgupta and P. K. Saha, "Eigenvalue spectrum of rectangular waveguide with two symmetrically placed double ridges," *IEEE Trans Microwave Theory Tech.*, vol. MTT-29, pp. 47–51, Jan. 1981.

[10] G. G. Mazumder and P. K. Saha, "A novel rectangular waveguide with double T-septums," *IEEE Trans. Microwave Theory Tech.*, vol. MTT-33, pp. 1235–1238, Nov. 1985.

[11] P. K. Saha and D. Guha, "New broadband rectangular waveguide with L-shaped septa," *IEEE Trans. Microwave Theory Tech.*, vol. 40, pp. 777–781, Apr. 1992.

Modal Scattering Matrix of the General Step Discontinuity in Elliptical Waveguides

Paweł Matras, Rainer Bunger, and Fritz Arndt

***Abstract*—In this paper, a direct mode-matching technique is proposed for the calculation of the modal scattering matrix of nonconfocal, twisted, and/or displaced step discontinuities in elliptical waveguides of different cross sections. For the convenient treatment of the Mathieu functions, an efficient trigonometric series expansion technique is used. As examples, the scattering parameters are calculated for typical step discontinuities demonstrating the flexibility of the method.**

***Index Terms*— Mode-matching methods, waveguide discontinuities, waveguide junctions.**

I. Introduction

For the analysis of the step discontinuity at elliptical waveguides, an efficient direct mode-matching technique has been recently proposed [5]. The investigation was limited to the simple case of confocal elliptic cross sections. The rigorous solution of the scattering problem at the general (nonconfocal, twisted, and/or displaced) discontinuity [see Fig. 1(a)], however, is required for the analysis of more complicated structures such as displaced elliptic irises or shaped horns. This paper presents, therefore, the extension of the direct mode-matching technique to this general case.

II. Theory

For a waveguide of elliptical cross section [cf. Fig. 1(b)] with the focal distance $2h$, the wave equation for the corresponding transversal eigenfunctions $T(\xi, \eta) = U(\xi)V(\eta)$ is given in elliptic coordinates ξ, η, z by [4]

$$\frac{\partial^2 V}{\partial \eta^2} + (a - 2q\cos 2\eta)V = 0 \tag{1}$$

$$\frac{\partial^2 U}{\partial \xi^2} - (a - 2q\cosh 2\xi)U = 0 \tag{2}$$

Manuscript received November 10, 1995; revised November 21, 1996.

The authors are with the Microwave Department, University of Bremen, D-28359 Bremen, Germany.

Publisher Item Identifier S 0018-9480(97)01730-4.